ELSEVIER

REVIEW ARTICLE

Interface Property Characterization and Strengthening Mechanisms in Fiber Reinforced Cement Based Composites

Victor C. Li* and Henrik Stang†
Advanced Civil Engineering Materials Research Laboratory, Department of Civil and Environmental Engineering, University of Michigan, Ann Arbor, Michigan and †Department of Structural Engineering and Materials, Technical University of Denmark, Lyngby, Denmark

The properties of the fiber/matrix interface are of primary significance for the overall behavior of fiber reinforced cement based composites. The present paper gives an overview of the current knowledge regarding characterization and engineering of the interface. First, different mathematical models for the characterization of interface properties are reviewed, including strength as well as toughness based models, and basic interfacial parameters are identified. Second, engineering tools are reviewed—primarily ways of increasing the fiber/matrix bond by applying various strengthening techniques, including introduction of fiber deformations, densification of the porous fiber/matrix interfacial transition zone, and fiber surface modification using plasma treatment. The strengthening mechanisms are quantified through basic interfacial parameters, and it is shown by reference to available experimental evidence that substantial improvements in the fiber/matrix bond can be achieved, opening up the field for further optimization of fiber reinforced cement based composites. Finally, gaps in the present knowledge are pointed out, identifying areas of future research in this area.
ADVANCED CEMENT BASED MATERIALS 1997, 6, 1–20.

KEY WORDS: Fiber reinforced cement based composites, Fiber/matrix interface, Mathematical characterization, Interfacial friction, Fiber deformation, Interfacial transition zone, Plasma treatment

The study of fiber/matrix interfaces in cement based composites is important for two reasons. The first involves the predictive capability of models of composite properties associated with interface debonding and fiber pull-out processes. These properties include all composite strengths, fracture energy, fatigue behavior, ductility, and energy absorption capacities. In addition, there is ample evidence that composite long-term durability is related to interface property change in some fiber composites. In short, all composite properties beyond the linear elastic range of deformation may be expected to activate the failure of the fiber/matrix interface if fiber failure is prevented. (In turn, fiber rupture is strongly influenced by the magnitude of the interface bond, together with fiber length and strength.) Hence, to predict these composite properties, it is necessary to characterize the interface failure mode and to supply the related parameter(s) to the composite model.

Another equally important reason for the study of fiber/matrix interfaces derives from the interest in improving the composite properties via tailoring of interfacial property. For this purpose, it is necessary to develop an appropriate test method for determination of interface property improvements. This is usually carried out by means of a single fiber pull-out test in which the load and load-point displacements are measured. These data are then used to deduce interface properties. Alternatively, interface properties can be inferred from measurable composite properties.

For either of these two reasons for interface study, it is necessary to have a constitutive model of fiber/matrix interface debonding and post-debonding sliding. In this article, we review some fundamental concepts of interface property characterization as well as three broad groups of techniques used for interface property improvements. This includes fiber deformation, interface transition zone modification, and fiber

Address correspondence to: Henrik Stang, Department of Structural Engineering, Technical University of Denmark, DKM, DTU, Bygning 118, 2800 Lyngby, Denmark.
Received January 17, 1996; Accepted February 29, 1997

ISSN 1065-7355/97/$17.00
PII S1065-7355(97)00004-7

surface modification. The purpose of this survey is to provide a comprehensive, consolidated, and up-to-date overview of various approaches in fiber/cement interface bond property tailoring. The existing information on this topic is rather scattered in the literature, and yet the subject is clearly gaining importance in systematic engineering of advanced cementitious composites. In treating this subject, we have attempted to cover most fiber types used in cementitious composites and emphasized the variety of mechanisms of strengthening in interfacial bonds. We have also included some of the latest advances based on our own research. It is a goal of this article to serve as a sound starting point for readers interested in pursuing research in tailoring of fiber/cement matrix interface in advanced cementitious composites.

The subject of fiber/cement matrix interface is much broader than the specific focus intended in this article. A general broad overview of fiber/matrix interfaces is given by Bentur et al. [1]. A concise summary of critical elements of interface microstructures can be found in a recent article by Bentur [2]. Gray and Johnston [3] reviewed single fiber pull-out testing techniques for interface property characterization. Interpretation of interface bond property based on bend-over point of composite tensile test can be found in Stang [4], that based on composite ultimate tensile strength can be found in Li [5], and that based on composite tensile stress versus crack opening relationship can be found in Li et al. [6] and Stang et al. [7].

The word interfacial "bond" in this article generally refers to either a chemical and/or mechanical bond. The text will make it clear when there is a need to differentiate the two.

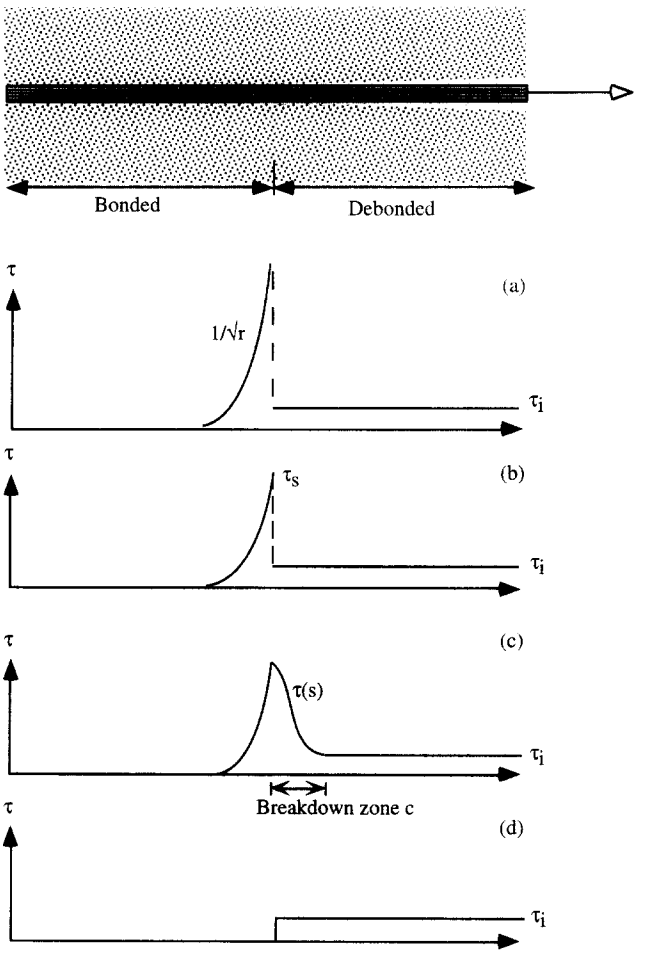

FIGURE 1. Interface property characterization corresponding to various assumed debond modes. (a) Linear elastic brittle fracture model; (b) cohesive strength model; (c) slip-weakening fracture model; (d) simplified strength model.

Fiber/Matrix Interface Characterization

Interface Strength versus Interface Toughness

A fundamental requirement of any interface debonding model is the prescription of a bond failure criterion. This means that when a certain debonding criteria is satisfied, the debond zone will advance, and the debonded zone is (generally) assumed to undergo frictional sliding at a constant stress τ_i. In most models, either a strength based criterion or a fracture based criterion is prescribed. Figure 1a shows a schematic of interface shear stress distribution for a fracture based debond model. The characteristics of such a linear elastic fracture model is that the shear stress at the tip of the debonded zone becomes unbounded, and that adequate energy must be supplied to the interfacial material at the debonded crack tip to drive the debond zone forward. This corresponds to the interfacial fracture energy. The fracture based debond model has been analyzed [8–10]. Interfacial fracture energy for steel/cement systems is on the order 10 to 20 J/m^2 [11,12]. This is comparable to the fracture energy of neat cement paste.

An alternative interface debond model is the strength based model in which the criterion for the debond zone to advance is that the interface shear stress must reach a critical value, termed the shear strength τ_s. The shear stress distribution for this model is schematically shown in Figure 1b. The interface in the debonded zone again slides under a constant frictional stress τ_i.

The infinite stress at the crack tip in the linear elastic fracture model is due to the assumption of elastic material behavior along the interface up to the debonded zone. More realistically, the shear stress τ gradually decays as the material breaks down under high localized shear deformation (Figure 1c). Such a breakdown zone concept was first proposed by Palmer and Rice [13] to describe the progressive advance of slip planes on overconsolidated soils under mode II type deformation. This slip-weakening concept should apply

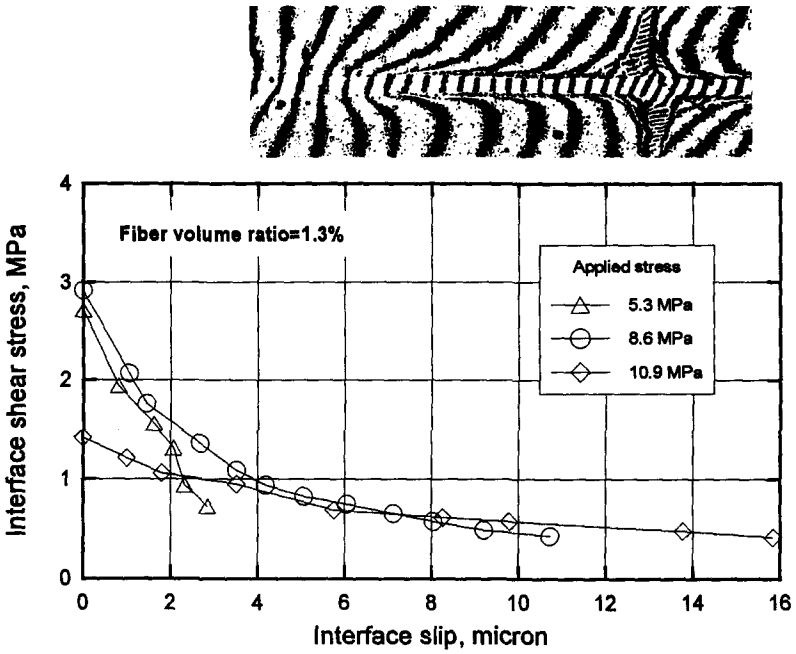

FIGURE 2. Slip-weakening $\tau(s)$ inferred from Moiré interferometry [15].

equally well to describe progressive debonding of the fiber/matrix interfaces. In the slip-weakening model, the shear stress makes a continuous transition (with no jumps) across the breakdown zone from the bonded to the debonded region. The dimension of the breakdown zone c is governed by the details of the shear stress versus slip relationship $\tau(s)$. Physically, it can be expected that the size of the breakdown zone will depend on the microstructural details of the interface for a particular fiber/matrix system (material and processing). In general, for coarse grained microstructures such as in most fiber reinforced cement based composites, the breakdown zone size can be large compared to in-plane dimensions, and the strength based case may be approached. However, special processing techniques and mix designs with refined microstructures may create situations where c is small and the linear elastic fracture based case may be approached as the classical "small scale yielding" limit is satisfied. Based on a J-integral analysis, Rice [14] showed that the fracture energy can be related to the $\tau(s)$ relationship:

$$\Gamma = \int_c [\tau(s) - \tau_i] ds, \tag{1}$$

where the integral above is carried over the length of the breakdown zone c. Note that τ and s generally vary from point to point along the breakdown zone. The slip-weakening model is analogous to the tension-softening model in Mode I crack in cementitious materials.

The constitutive relationship between τ and s on the interface is usually difficult to determine. However, Shao et al. [15] did infer such a relationship from Moiré interferometry (Figure 2) for a steel/cement composite system. From this data and eq 1, the interface fracture energy can be estimated to be approximately 8 J/m^2. This appears to be consistent with estimates made from single fiber pull-out tests mentioned earlier. (The residual frictional stress, measured at about 0.5 MPa [15], may be a lower bound of the actual value due to the preparation procedure of the specimen. Surface grinding to partially expose the fiber to surface deformation mapping may release part of the radial stress induced by shrinkage strain responsible for the Coulomb friction, see further discussion on shrinkage strain, to follow. Deduction by inverting measured gross composite properties puts the interfacial bond at upwards of 4.5 MPa). The size of the breakdown zone c based on Moiré interferometry measurement is on the order of 1 to 2 mm. This is a relatively large length considering that the total debond zone was only on the order of 4 mm. The common assumption of small scale yielding at the crack tip in linear elastic fracture mechanics cannot be valid in this case. The slip-weakening model (Figure 1c) may be needed to accurately describe the debonding process.

In some cementitious composites, chemical bonding (or sometimes referred to as elastic bonding) between the fiber and matrix is not strong in comparison to frictional resistance along the debonded segment against pull-out. For the strength based model, this means $\tau_s = \tau_i$. For the fracture models, no chemical bonding implies $\tau(s) = \tau_i$ or $\Gamma = 0$ in eq 1. In such cases,

the bonded part of the interface and, thus, the debonding criterion become unimportant. In general, friction plays a more and more important role with increasing fiber size and increasing confining stress (lateral constraint). The whole interface can then be thought of as unbonded and the fiber/matrix held together by friction. When a load is put on the fiber end, a frictionally activated interface segment with $\tau = \tau_i$ provides resistance to sliding against the applied loads (Figure 1d). This is the most commonly adopted assumption in bond strength determination from the fiber pull-out test. The simplicity of this assumption also makes it widely adopted in micromechanical models of composite properties in which the debonding of interfaces is explicitly accounted for.

The issue of the nature of the interface bond was experimentally examined by Li and Chan [16] by interpreting the pull-out force P of steel and brass fibers in cement matrix through the following generalized debonding model:

$$P = f(\delta; \tau_{eff}, d_f, l), \tag{2}$$

where δ is the fiber exit-point displacement, and d_f and l are the fiber diameter and embedment length, respectively. Specific forms of eq 2 have been given [9,17,18], all based on shear lag analyses, for slightly different boundary conditions of the fiber pull-out problem. These forms are good for both strength based debonding and fracture based debonding. The interface parameter τ_{eff}, however, has different meanings [16,19] (see also Stang et al. [17] for comparison):

$$\tau_{eff} = \begin{cases} \tau_s & (strength\text{-}controlled) \\ \tau_i + \sqrt{\dfrac{2E_f\Gamma(1-\alpha)\rho^2}{d_f}} & (fracture\text{-}controlled) \end{cases} \tag{3}$$

For the strength based model, τ_{eff} is simply the shear strength τ_s. For the fracture based model, however, τ_{eff} is related to the interfacial fracture energy Γ, the fiber volume fraction V_f (through the parameters α and ρ), and the fiber stiffness E_f and diameter d_f. This suggests that if τ_{eff} is obtained from a pull-out test of the same fiber type with different diameters and found to remain constant, then the debonding process is likely controlled by interfacial strength. Otherwise, the debonding is likely controlled by interfacial fracture energy.

The parameters α and ρ are defined in terms of fiber and matrix elastic stiffness, volume fractions, and average fiber spacing. Details can be found in Li and Chan [16].

Li and Chan [16] showed that, for steel and brass fiber/matrix systems, with diameter varying from 0.4 to 1 mm, τ_{eff} remains essentially constant at 3.8 and 4.6 MPa, respectively (Figure 3). They concluded that the interface debond processes are governed by strength rather than fracture. Indeed, in those particular fiber/matrix systems, no sudden load drop occurs at peak pull-out load, suggesting that $\tau_s = \tau_i$. This result indicates that use of the simplified interface stress characterization denoted in Figure 1d may be justified, at least for fiber composite systems comparable to those investigated by Li and Chan [16].

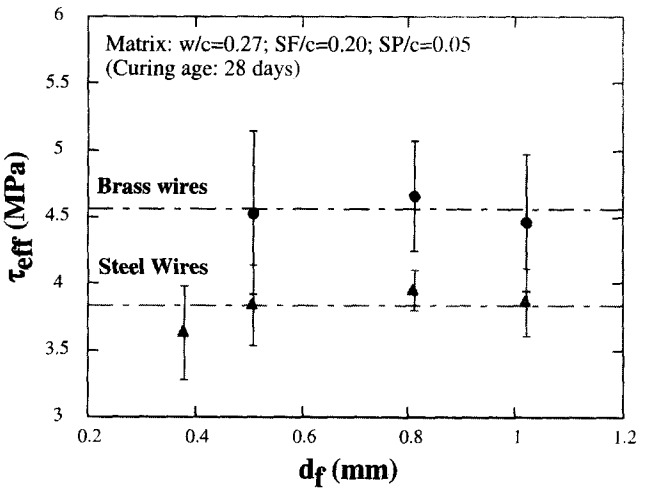

FIGURE 3. Measured τ_{eff} shown to be independent of fiber diameter (d_f) for steel/cement and brass/cement system [16].

In the study by Shao et al. [15], the authors reported an increase of interface bond from 4.5 to 7.5 MPa when the fiber volume fraction was increased from 1.3% to 5.9%, inferred from the first crack strength measured in these composites and using the ACK [20] steady-state crack model. This increase of bond strength τ_{eff} with fiber volume fraction is expected from eq 3 and suggests that, for this system, the interface is governed by a fracture-like mode of debonding.

Interface Friction

The residual frictional stress τ_i has usually been assumed to be a material constant, resulting in a straight descending line for the post-peak P-δ relationship corresponding to fiber pull-out. However, there is increasing evidence to suggest that this parameter may be modified by damage processes either in the fiber or in the matrix as the fiber undergoes slippage in the post-debonding stage. Fibers not ruptured are expected to slide out in the crack wake with larger crack opening in the fracture of a composite specimen. Thus, the possible slip-dependence of τ_i must play an important role in composite fracture energy [21] and in bending strength [22]. In polymeric fibers that have low lateral strength, fiber damage may occur during sliding by surface abrasion (Figure 4). This in situ fibrillation

FIGURE 4. Surface abrasion of nylon fiber pulled out from a cement matrix [66].

process during fiber pull-out causes jamming of the fiber and results in higher pull-out load. Experimental evidence is available on polypropylene fibers and nylon fibers [23,24] and on high modulus polyethylene fibers [25]. To account for this slip-dependence, Wang et al. [23] found it necessary to modify the constant τ_i to the form:

$$\tau_i = \tau_o + a_1 s + a_2 s^2, \tag{4}$$

where the values of τ_o, a_1, and a_2 for the nylon and monofilament polypropylene fibers can be found in Table 1. The resulting slip-hardening relationship appears to provide a good fit to data of two-sided fiber pull-out experiments (Figure 5).

For straight steel fibers in cement matrix, the pull-out curve is usually concave upward, suggesting a damage process on the matrix or transition zone as slip increases, which results in a more compacted microstructure and possible reduction of surface contact between the fiber and matrix. This has been confirmed recently by scanning electron microscopy (SEM) and energy-dispersive X-ray (EDX) analyses [24] on the mortar surface after steel fiber debonding and sliding out. Furthermore, it can be argued [26] that if a fiber-matrix misfit is present due to shrinkage of the matrix and results in contact pressure related frictional stresses, the compaction of the interfacial microstructure will lead to gradual decay of the misfit and thus a gradual decay of the frictional stresses. The use of τ_o, a_1, and a_2 values in Table 1 for straight steel fibers results in good fit to experimental data (Figure 6). Unlike the polymeric fibers, straight steel fibers have a slip-softening effect reflected by the negative coefficient a_1 in eq 4.

Although the frictional stress dependence on slip represented by eq 4 shows resemblance to the slip-weakening concept of $\tau(s)$ discussed in the previous section in connection with debonding mode and characterization, the basic physical concepts and magnitude of slip s to activate the slip-dependent friction and breakdown mechanisms are very different. For example, in the Moiré interferometry study of Shao et al. [15], the strength degradation rate in the breakdown zone

TABLE 1. Interface data (eq 4) inferred for various fiber types and matrices

Fiber	[Ref]/Mix	τ_o (MPa)	a_1 (MPa/mm)	a_2 (MPa/mm^2)	Slip Range s (mm)	Figure No.
Single Fiber Pull-Out Test						
Nylon	[23]	0.05	0.001	0.0002	50	5a
Monofilament polypropylene	[23]	0.1	0.0005	0.0003	50	5b
Straight steel	[23,64]	2.35	−0.35	0.014	12.7	6
Composite Tensile Test						
Fibrillated polypropylene	[6]/8500/Fatigue-5	0.8	0	0	0.3	12, 15, 16
Straight steel 25/0.4	[6]	4.2	−4.0	1.0	0.3	13
Straight steel 12.5/0.4	[7]	6.0	−4.0	1.0	0.3	—
Straight steel 25/0.4	OB-10	2.9	−4.0	0	0.3	—
Hooked steel 30/0.5	ZB-05	3.5	4.0	−10.0	0.3	14
Hooked steel 30/0.5	8500	3.5	4.0	−10.0	0.3	15
Hooked steel 30/0.5	Fatigue-5	4.5	−2.0	0	0.3	16

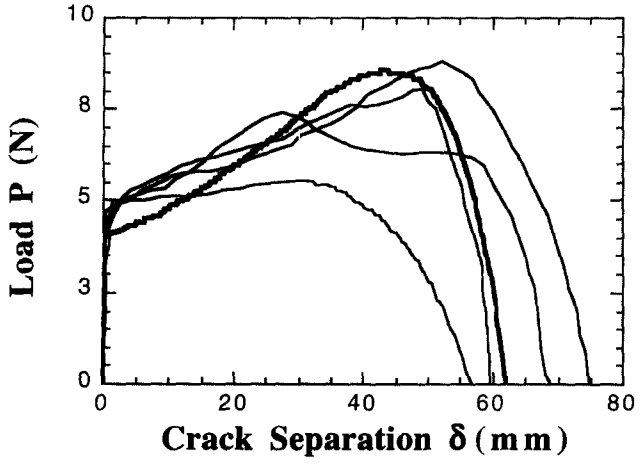

(a)

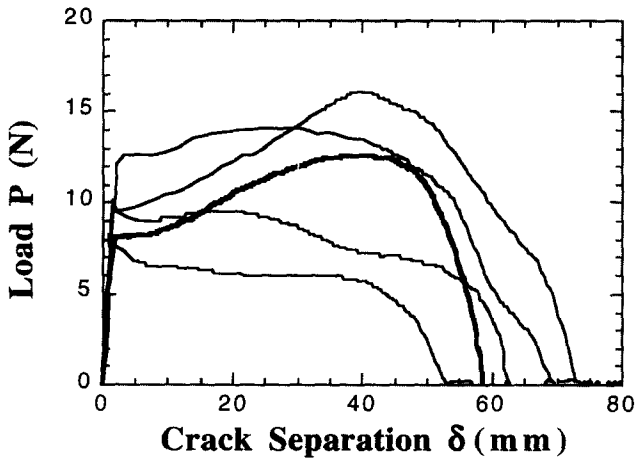

(b)

FIGURE 5. Measurement and slip-dependent friction model (heavy lines) of two-sided (a) nylon and (b) polypropylene fiber pull-out test [23].

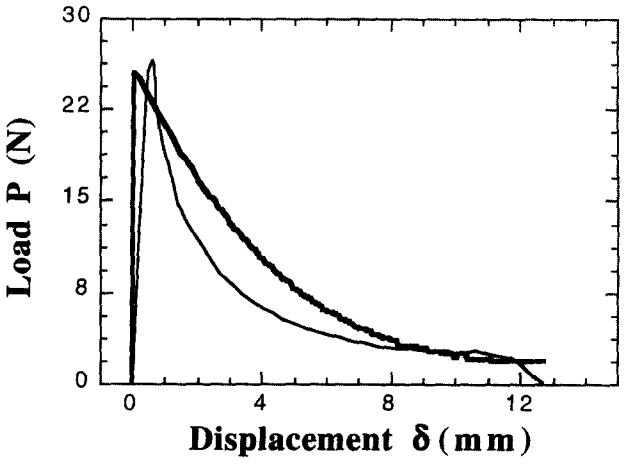

FIGURE 6. Measurement and slip-dependent friction model (heavy line) of one-sided steel fiber pull-out test [23].

(eq 1, see also Figure 1d) amounts to approximately several MPa/μm (or 10^3 MPa/mm), whereas the value of a_1 (in eq 4) is on the order of MPa/mm or less for most material systems studied. The breakdown mechanism is essentially a new surface creation process and is therefore directly associated with the fracture energy of the interface as discussed in connection with eq 1. The slip-dependent friction in eq 4 is related to the damage suffered by fiber or the surrounding cement groove in previously existing contact surfaces in frictional sliding.

The fundamental issue of what gives rise to τ_0 in eq 4 has not been adequately addressed, even for straight smooth fibers. This is an important issue, particularly for developing an appropriate strategy for interface property modifications, as will be discussed in the next section. There is evidence that τ_0 may be sensitive to lateral pressure. For example, Leung and Geng [27, 28] developed an ingenious method of testing fiber pull-out under variable normal stress and found that τ_0 obeys a Coulomb-type friction law with coefficient of friction μ:

$$\tau_0 = \tau_0' + \mu\sigma_n^{sh} + \mu\sigma_n^{ext}. \tag{5}$$

The first term may be interpreted as the friction of the contact surfaces without any residual normal stress due to shrinkage (second term) or external normal stress (third term). For the steel fiber with diameter of 0.5 mm, Leung and Geng [27,28] found that $\tau_0' + \mu\sigma_n^{sh} = 4.5$ MPa and $\mu = 0.15$. This Coulomb-type friction is supported by similar findings of Pinchin and Tabor [29] and Kim et al. [30]. On a composite level, Li et al. [31] also found that the tensile failure strength under biaxial tension-compression loading is higher than that of uniaxial tensile loading for the same polyethylene fiber reinforced cement based composite. Presumably, the lateral compressive stress leads to a higher reinforcement efficiency due to enhanced interfacial bond strength τ_0 magnified by the Coulomb friction effect (via the term $\mu\sigma_n^{ext}$ in eq 5).

If τ_0 is sensitive to lateral pressure, it would seem reasonable to expect that its magnitude may be affected by the shrinkage of the surrounding cementitious matrix during composite curing. A large shrinkage of the matrix or high elastic modulus of the fiber should produce a high lateral pressure on the fiber. This concept was recently investigated by Stang [32]. It is reasonable to expect that the coefficients a_1 and a_2 in the slip-dependent friction description of eq 4 may also be dependent on normal stress and therefore the matrix shrinkage effect. However, there are no data at present to confirm or disprove this dependence.

In Stang's [32] report, a laboratory mercury thermom-

TABLE 2. Predicted clamping pressure σ_n^{sh} and frictional shear stress τ on fiber/matrix interfaces in cement paste with water/cement ratio 0.3 containing 0 or 10% microsilica (ms) at 500 hours after curing at 20°C, elastic constants for the fiber E and ν, and frictional coefficients of the fiber/matrix interfaces μ

Fiber Type	E (GPa)	ν	μ	σ_n^{sh} (MPa)		τ (MPa)	
				0% ms	10% ms	0% ms	10% ms
Steel	210	0.3	0.05–0.25	6.4	19	0.3–1.6	1.0–4.8
Carbon	240	0.2	0.05–0.1	5.9	17	0.3–0.6	0.9–1.7
Polypropylene	1	0.4	0.3–0.5	1.1	3.1	0.3–0.6	0.9–1.6

eter was used as a pressure sensor and embedded into a cylindrical block of cement paste. In this way it was possible to make direct measurements of the clamping pressure induced by the autogenous shrinkage of the cement paste as a function of time. By knowing the overall stiffness of the thermometer and the elastic moduli of the cement paste during hydration, an effective shrinkage can be computed as a function of time by modeling the thermometer as an equivalent ellipsoidal inclusion. This information, combined with known elastic moduli of any fiber and using again the solution for an ellipsoidal inclusion, leads to estimates of the time-dependent normal pressure σ_n^{sh} and the Coulomb-type friction on the interface. The calculated interfacial friction that accounts only for the second term $\mu\sigma_n^{sh}$ in eq 5 is shown in Table 2 for steel, carbon, and polypropylene fibers embedded in two different matrices—cement paste with and without microsilica (condensed silica fume)—known to exhibit very different autogenous shrinkage. Remarkably, these values are close to those typically measured in fiber pull-out tests of corresponding fiber types and matrices, suggesting that the dominant contribution of interfacial friction is due to cement shrinkage and fiber elastic stiffness. Further, the effect of different amounts of matrix shrinkage is shown. The matrix with microsilica exhibits three times as high free autogenous shrinkage after 500 hours as the matrix without microsilica, resulting in an increase of Coulomb-type friction on the same order of magnitude.

These results to some extent question the usual assumption that microsilica increases bonding properties solely due to densification effect of the interfacial transition zone (see the following section on transition zone modification). Finally, since the effective shrinkage depends heavily on environmental conditions such as temperature and humidity, the results of this investigation underline the importance of controlling environmental conditions during testing of interfacial properties and including environmental conditions in the modeling. At present this has not been done in any systematic way.

Strengthening Mechanisms

A variety of interface bond strengthening mechanisms have been proposed and utilized. Some of these make use of macroscopic processes such as fiber deformation. Others utilize microscopic changes such as fiber surface and/or interface transition zone modifications. These three broad classes of interface bond strengthening techniques are summarized here. Table 3 collects information on effects on interface properties due to various strengthening mechanisms for a number of fiber types.

Fiber Deformation

Most fiber deformation processes result in an increase in surface area of contact with the cement matrix per unit fiber length. In addition, most fiber deformation processes lead to local mechanical interactions between fiber and matrix on the millimeter scale and, therefore, may be regarded as a macroscopic "roughening" effect. Hence, the effective "interface" bond property must be interpreted in this larger scale context.

One of the earliest techniques used to modify the interfacial bond between polymeric fiber and cementitious matrix is by means of fiber fibrillation [33–35]. A photograph of fibrillated polypropylene fibers is shown in Figure 7. Fibrillation is carried out by comb-like cutting of an extruded and stretched thin film of the polypropylene material. The fibrillation process achieves two aims: it increases the specific surface area of contact and enhances mechanical anchorage to the cement matrix, as well as improving the fiber modulus. Krenchel [34] indicated that a factor of 3 or more can be achieved in bond strength improvement when the fiber has been fibrillated.

Another technique to improve mechanical anchorage and therefore bonding to a cementitious matrix is by twisting the fibers. Naaman et al. [36] reported that an increase in interfacial bond by a factor of 7 (compared with untwisted straight fibers) can be achieved by this method. Figure 8a shows a photograph of two-ply twisted polypropylene fibers. The effect of fiber twisting on the pull-out curve is shown in Figure 8b.

The fibrillation and twisting deformation processing

TABLE 3. Strengthening mechanisms and effect on interface properties

Fiber Type	Strengthening Mechanisms	Effect on Interface Properties	Reference
Polypropylene	Fiber fibrillation	Bond increase by factor of 3	[34]
Polypropylene	Fiber twisting	Bond increase by factor of 7	[36]
Nylon	Fiber crimping	Bond increase by factor of more than 6	[37]
Steel	Fiber crimping	Effective bond increase by factor of 1.4–10.5 depending on matrix type*	[38]
Steel	Fiber hooked end	Effective bond increase by factor of 2.8–27.6 depending on matrix type*	[38]
Steel	Fiber hooked end	Slip hardening (Table 1)	This study
Brass	Interface densification	Bond increase by 18% in microsilica matrix with low w/c ratio	[50]
Steel	Interface densification	Post-peak slip-dependence reduced	[50]
Steel	Interface densification	Bond increase by factor of 2 using a Densit matrix	[53]
Steel	Interface densification	Bond increase by a factor of 2.3 using a DSP matrix	[55]
Carbon	Interface densification	Bond increase by 95% using microsilica matrix with low w/c ratio	[56]
Steel	Interface densification	Bond increase by 60%–80% by addition of 1.4% by weight of PVA	[58,59]
Steel	Interface densification	Bond increase by factor of 4 by addition of 15% by weight of acrylic polymer particles	[45]
Polyethylene	Plasma treatment	Bond increase by 50%–100%; factor of six increase demonstrated	[62,63]
Polypropylene	Plasma treatment	Slip-hardening	[25]

*Bond improvement better represented by eq 4.

are particularly suitable for polymeric fibers due to its low strength and large strain capacity. They are not usually applied to higher strength materials such as steel fibers or brittle materials such as carbon fibers. However, the crimping process has been applied to both polymeric and steel fibers. Li et al. [37] showed that the pull-out process can be significantly altered by mechanically crimping a nylon fiber (Figure 9). For this case an improvement of the effective bond strength of more than six times has been achieved. The mechanical bond was so strong that pull-out of the fiber was limited by the strength of the nylon fiber. The effect of crimping on steel fibers (Figure 10) was studied by Banthia [38]. He reported increases in peak pull-out load in the range of 1.4 to 10.5 times that of straight fibers (with same diameter, cross-sectional shape and embedment length) depending on the type of matrix material with different water/cement (w/c) ratio, sand, and microsilica contents. The upper end of this peak load increase is likely limited by the fiber strength, resulting in fracture of the crimped fibers in the denser matrix.

FIGURE 7. Fibrillation of polypropylene fiber to enhance mechanical bonding.

Most steel fibers used for cement based composites are deformed. Apart from crimp deformation, another common type of deformation is creation of a hooked end (Figure 11a). Presumably, the initial stage of debonding for this type of fiber would not be different from that of straight fibers. However, when debonding reaches the hook, plastic deformation of the fiber and local crushing of the matrix may occur before the fiber can be drawn out. This results in an alteration of the effective bond. Two-sided pull-out of single fibers (Fig-

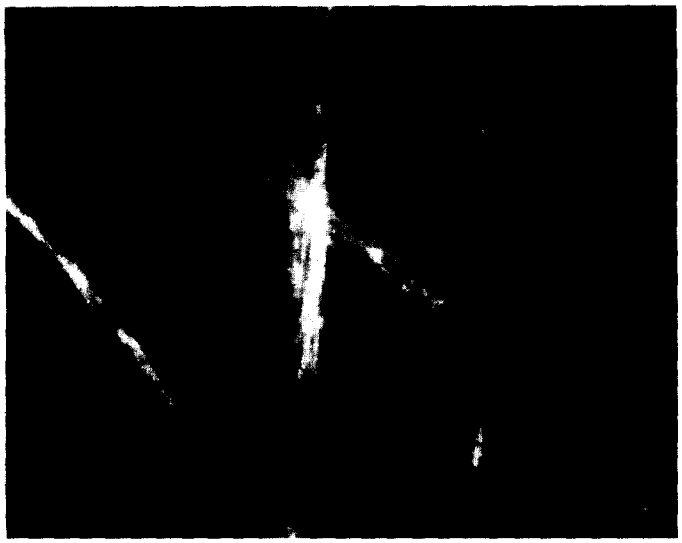

(a)

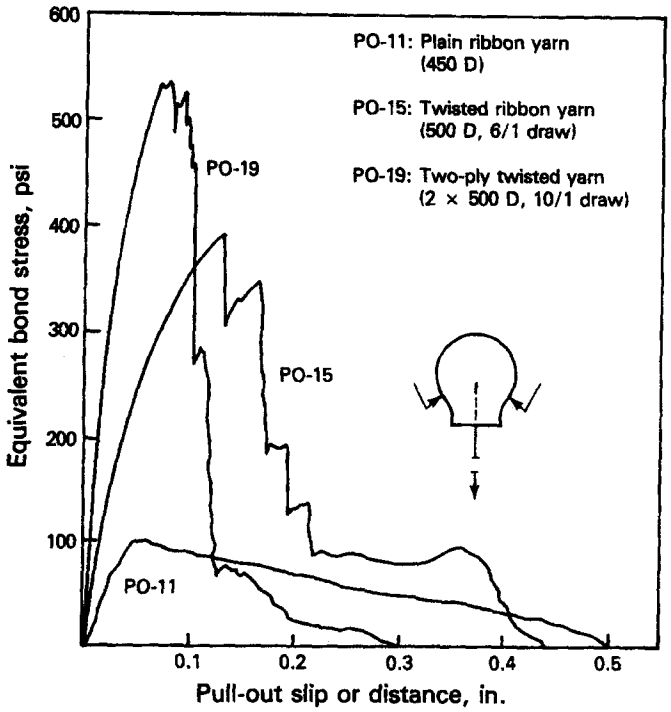

(b)

FIGURE 8. (a) Photograph and (b) pull-out test curves for twisted polypropylene fibers [36].

ure 11b [38]) suggested an increase by a factor of 2.8 to 27.6 in maximum pull-out load in comparison with that of straight undeformed fibers, again depending on the type of matrix material.

The reported increase in peak pull-out load for the crimped and hooked end steel fibers can be interpreted as an enhancement of the effective interface bond property. However, using the bend-over point of the single fiber pull-out versus displacement curve, Banthia and Trottier [39] found that the interfacial bond strength for deformed fibers was 2 to 8 MPa, with the higher end associated with those fibers embedded in a high strength matrix. The peak load can be several times higher than the load at the bend-over point and is dependent on the steel property. Depending on the deformed shape, the peak load may occur at very large slip values, up to a couple of millimeters. As is shown below, the effect of a hooked end on interface bond property may be more phenomenologically represented by the slip-dependent-type interface model described in eq 4.

Apart from the single fiber pull-out test, the interface bond property can also be deduced from uniaxial tensile composite tests in which the tensile stress versus crack opening relationship was continuously monitored. An assumption has to be made that the interface slippage s in eq 4 can be approximated by the crack opening w. With this assumption, and accounting for the Cook-Gordon effect, as well as the random fiber distribution and orientation effect, Li et al. [6] and Stang et al. [7] modeled crack opening versus tensile stress, which compares favorably to that determined from composite tensile experimental tests. It is possible to capture the σ–w relation for different fiber volume fractions up to 3% (Figures 12 and 13) with a single set of values of τ_o, a_1, and a_2, also listed in Table 1 for fiber reinforced concretes (FRCs) containing fibrillated polypropylene fibers and for FRCs containing straight steel fibers. The same procedure has been applied to FRCs containing deformed steel fibers with hooked ends (Figure 14). The σ-w curve for FRCs with a hybrid fiber system can be predicted based on the deduced τ_o, a_1, and a_2 from FRCs with a single fiber type (Figure 15). As expected and noted earlier, the interface parameters must depend not only on fiber type, but also on the matrix property. This is illustrated in Figure 16, which shows the measured and modeled σ-w curves for an FRC with the same hybrid fiber system but with a matrix different from that for the FRC just described (Figure 15).

Details regarding mixing and testing of the mixes referred to in Li et al. [6] and Stang et al. [7] can be found in Stang and Aarre [40] and Hansen and Stang [41]. For details regarding mixing and testing of mixes OB-10, ZB-05, and 8500, see Hansen and Stang [41] Mix Fatigue-5 is described in Stang and Jun [42]. The interfacial parameters used in Li et al. [6] and Stang et al. [7] and all the present investigations are summarized in Table 1. The composition for all mixes are summarized in Table 4.

It is evident from the figures that the polynomial shear stress/slip relation (eq 4) is able to describe pull-out of both straight and hooked steel fibers. For the steel fibers, the first term τ_o seems to be fairly constant

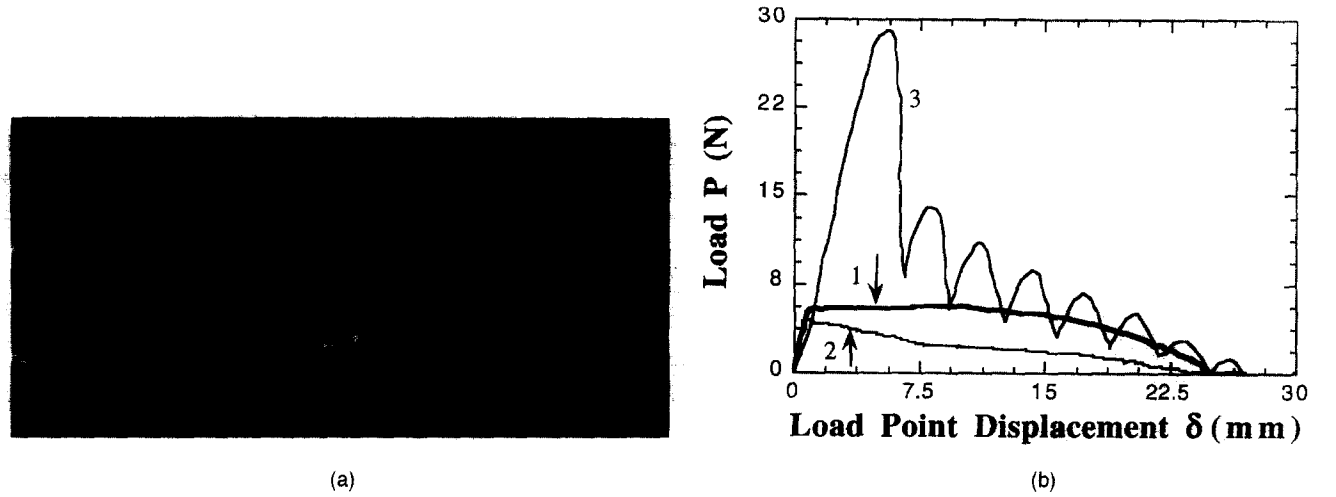

FIGURE 9. (a) Photograph of a crimped nylon fiber, and (b) pull-out test curves for nylon fiber with different surface treatments: (1) no treatment; (2) coated with fluorocarbon dry lubricant; (3) crimped and coated with fluorocarbon dry lubricant [37].

in comparable mixes: 2.9 to 4.2 MPa in all mixes except in Stang et al. [7], which is one with very low w/c ratio and with some cement paste replaced by microsilica and clay. The straight steel fibers exhibit slip softening in the crack opening range investigated, with a negative coefficient a_1 and with a negligible coefficient a_2. This result is consistent with the bond property determined from the single fiber pull-out test [23] as discussed earlier. For the hooked end fibers, the positive coefficient a_1 indicates a slip-hardening effect. Softening (negative a_2) does occur at larger slip values. An exception to this rule is the mix Fatigue-5, which shows slip softening even for hooked fibers. A possible explanation for this phenomenon could be extensive matrix cracking around the hooked ends in this relatively weak mix with larger w/c ratio (Figure 17).

It should be noted that the values of a_1 from the composite tests appear to be much larger than those from the single fiber pull-out tests (−4.0 versus −0.35, Table 1 for straight steel fibers). Part of the reason may be due to the difference in the range of sliding distance s. For the single fiber pull-out test, the coefficients for the τ-s relationship is fitted over the complete pull-out curves (Figures 5 and 6), involving a sliding distance of the length of the embedded fiber, typically in the range of millimeters. On the other hand, the coefficients for the τ-s relationship have been chosen to fit the composite crack opening w in the range of 0 to 0.3 mm. Thus, the magnitude of a_1 and a_2 is sensitive to the range of s of interest. It is likely that slip softening may be very rapid in the initial sub-millimeter range when the damage of the matrix around the fiber is most severe.

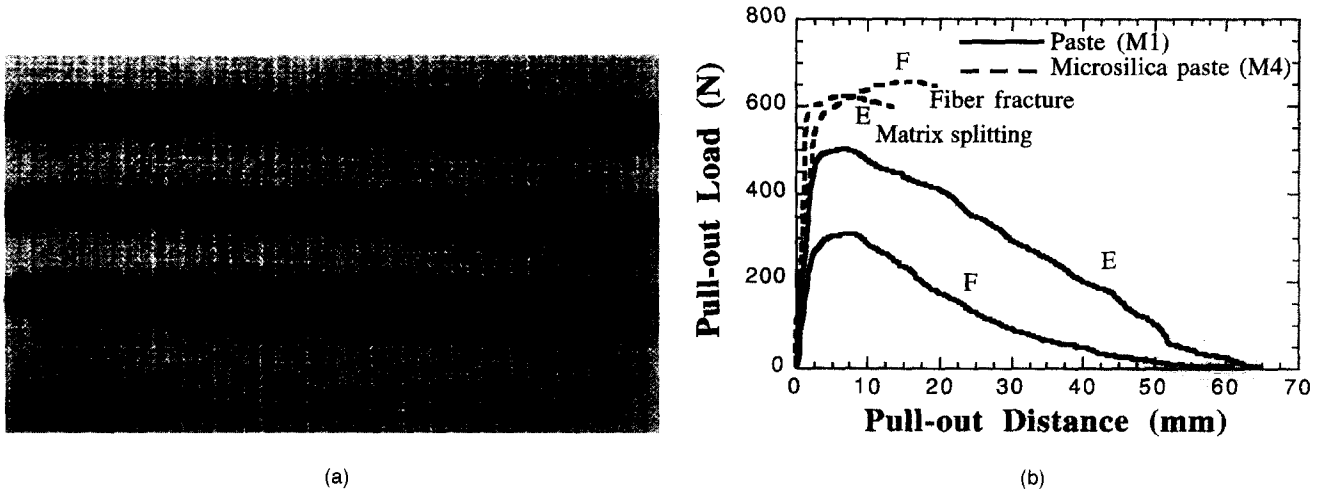

FIGURE 10. (a) Photograph and (b) pull-out curves for crimped steel fibers [38]. *E* and *F* are two different types of crimped fibers. Matrix (M4) has higher strength than (M1).

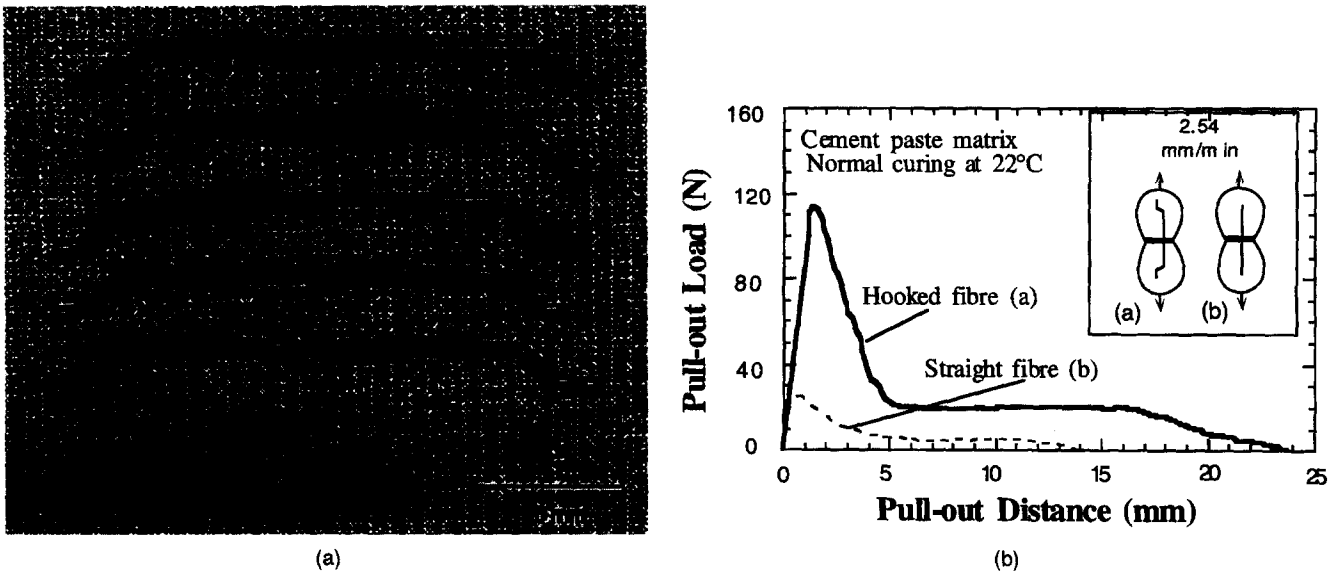

FIGURE 11. (a) Photograph and (b) pull-out curves for hooked end steel fibers [38].

This kind of behavior was observed by Naaman et al. [26], who used an exponential function to describe the frictional decay. Further, Rasmussen and Stang [43] observed that the initial portion of the τ-s relationship ($s < 0.1$ mm) cannot be described using the second-degree polynomial relationship.

Fiber deformation appears to be an effective strengthening mechanism for interfacial bond via modification of the coefficient a_1 and a_2 in the slip-dependent bond strength represented by eq 4. The magnitude of improvement depends not only on the fiber strength, but also on the strength of the surrounding bulk matrix due to the interaction with fiber anchorage. For some deformed fibers, the anchorage activation may exert itself strongly only after complete fiber debonding.

Transition Zone Modification

The presence of an interfacial transition zone (ITZ) between fibers and bulk matrix in cementitious composites has been confirmed by SEM [44], microhardness measurement [45], fluorescence microscopy [46], and Moiré interferometry [15]. Although the size of the ITZ varies with fiber type and fiber size [1] and matrix details, most observations suggest a relatively large porous and weak layer on the order of 40- to 70-μm thickness. The ITZ is generally assumed to be the weak link among constituents governing composite properties. Thus, it is expected that densification of the ITZ may serve to strengthen the transition zone and enhance the fiber/cement interfacial bond strength [47–49].

Chan and Li [50] investigated the effect of transition zone densification on the improvement of the bond strength between fibers and cement matrix of various fiber reinforced cementitious composites. The microstructure of the fiber/matrix transition zone was densified through the reduction of w/c ratio and the use of microsilica. ITZ densification was confirmed by direct observation of the cement groove after fiber peel-off using an environmental scanning electron microscope (ESEM). Bond strengths were measured based on single fiber pull-out tests of steel, brass (*not* brass-coated steel), and polyethylene fibers.

From the ESEM study, it was found that the compactness of the microstructure of the transition zone was much improved by reducing w/c ratio and/or using microsilica, regardless of fiber type. However, improvement in fiber/cement bond strength was found to depend on fiber type. Figure 18 shows the results of the single fiber pull-out tests for the steel fibers. Base on the peak load measured, no improvement was seen in the interface bond strength with matrix densification. However, the post-peak branches appear to respond to matrix densification effect (Figure 19), suggesting a reduction in the softening rate (and resulting in less matrix material damage) with sliding (i.e., a smaller negative a_1 value in eq 4). On the other hand, bond strength improvement for brass/cement system can be clearly detected for Matrix III (w/c = 0.27, SF/c = 0.2, SP/c = 0.05), which uses a lower w/c ratio than Matrix I (w/c = 0.4), and also includes microsilica, which is not used in Matrix II (w/c = 0.27).

The research findings of Chan and Li [50] indicate that transition zone densification does not always result in bond strength improvement. Similar conclusions were drawn by Glavind [51] and Glavind and Stang [52], when microsilica and clay were used as microfill-

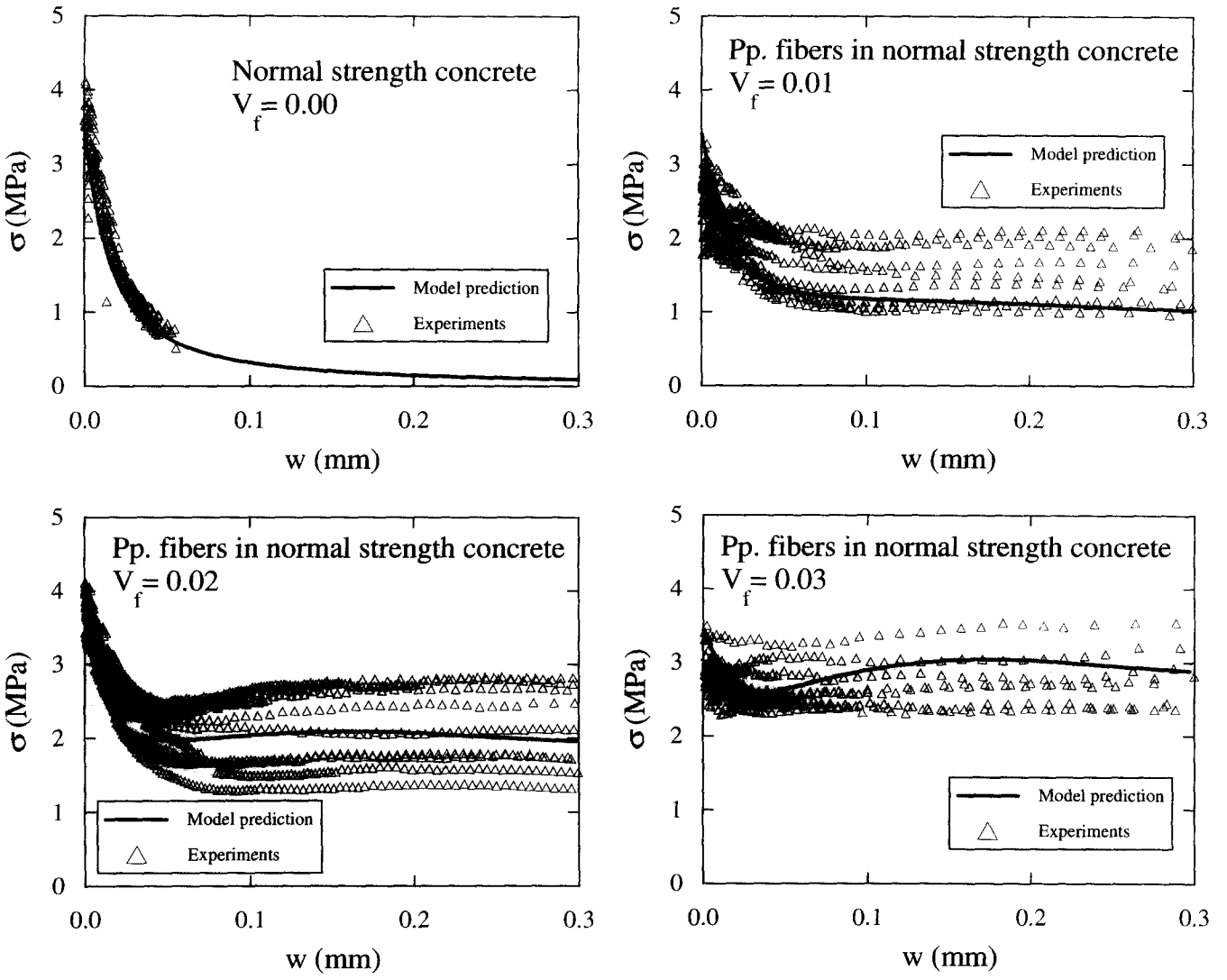

FIGURE 12. σ-w Relation from experimental measurement compared with model based on eq 4 for various fiber volume fractions [6] of fibrillated polypropylene fibers.

ers in steel fiber/cement matrix systems. Moreover, the ESEM observations [50] revealed that bond failure between steel or polyethylene fibers and cement matrix is of adhesive type, i.e., debonding took place at the contact surface between fiber and cement. On the other hand, the brass/cement bond strength increased with the density of cement matrix and the corresponding fiber debonding took place mainly in the heterogeneous transition zone. These findings indicate that the debonding of brass/cement system is related to failure inside the ITZ. Therefore, the brass/cement bond strength, which depends on the strength of the transition zone, is sensitive to matrix packing density. In contrast, the steel/cement and polyethylene/cement bond strengths apparently are dominated by the adhesion property between steel or polyethylene fibers and the adjacent cement material and are negligibly affected by the microstructure of the ITZ. As a result, transition zone densification may not be effective for bond improvement in the case of steel and polyethylene fiber reinforced cementitious composites.

Despite the discussion above, there appears contradictory evidence that when very carefully graded and densified matrix is used, as in a Densit material developed at the Danish Cement Factory Aalborg Portland, interface bond strength can increase in steel fibers. The Densit materials are characterized by a high amount of microsilica (typically about 20%) and a high amount of superplasticizer. The superplasticizer allows casting of these materials with a very low water-to-powder ratio (as low as 0.18). Recently, Nielsen [53] conducted some basic investigations on the mechanical properties of steel fiber reinforced Densit materials including determination of the σ-δ relationship for one typical Densit

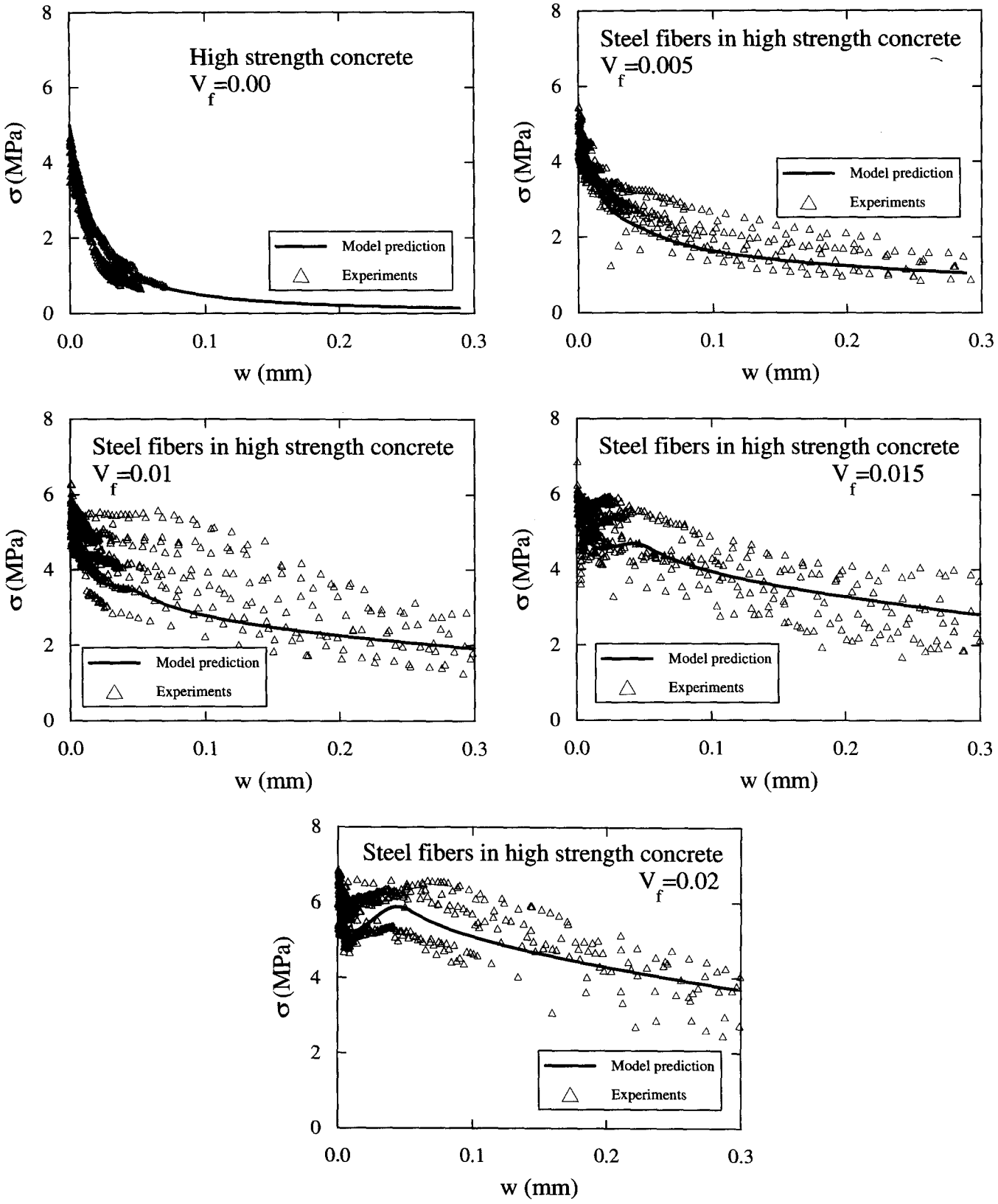

FIGURE 13. σ-w Relation from experimental measurement compared with model based on eq 4 for various fiber volume fractions [6] of straight steel fibers.

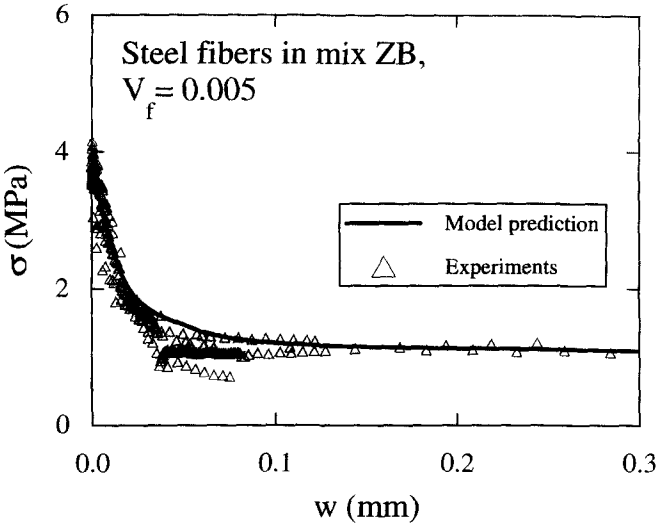

FIGURE 14. σ-w Relation from experimental measurement compared with model based on eq 4 for hooked end fibers.

matrix and seven different reinforcement types. The composition of the matrix material is given in Table 5, and an overview of the different types of reinforcement used in the investigation is given in Table 6.

To estimate the bonding parameters τ_o, a_1, and a_2, the model developed by Li et al. [6] and Stang et al. [7] was applied to describe the σ-δ relationship for the different types of fiber reinforcement. It turned out, however, that even though the peak stress can be predicted as a function of the fiber volume concentration based on a single set of bond parameters for each fiber type, the shape of the σ-δ relationship is inaccurately described by the model for the very high fiber volume concentrations. Typically the crack opening at peak load predicted by the model is too small. The reason for this discrepancy could be that not a single but several cracks are formed, even though the specimen is notched. Multiple cracking of notched specimens of similar size and shape has previously been observed in ordinary fiber reinforced concrete with 3 vol.% steel fibers by Aarre [54]. Obviously, the tendency toward multiple cracking increases with higher volume concentrations, which explains the growing discrepancy with the single crack model. Alternatively, it is possible that local matrix spalling under inclined bridging fibers is responsible for the additional crack opening. It is expected that this mechanism could be intensified when fiber volume fraction is high and fiber spacing is low, resulting in a "plug pull-out" mechanism. The bonding parameters deduced are summarized in Table 7. Throughout the investigation, the snubbing coefficient and the Cook-Gordon parameter [6] was set as follows: $f = 0.75$ and $\alpha = 15d_f$.

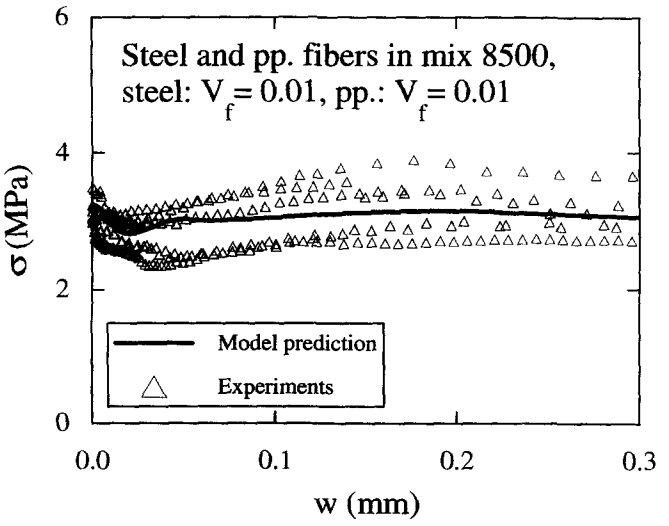

FIGURE 15. σ-w Relation from experimental measurement compared with model based on eq 4 for a hybrid composite containing hooked end steel and fibrillated polypropylene fibers.

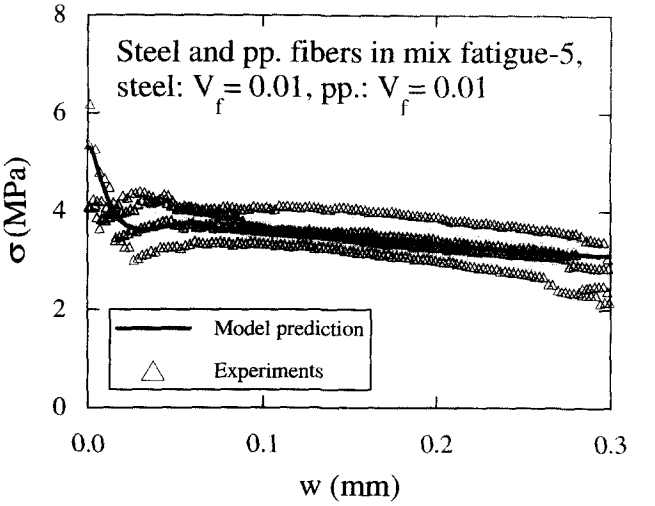

FIGURE 16. Same as Figure 15, but for a different matrix.

Several interesting points can be made by comparing the bond parameters for steel fibers in the Densit matrix with the bond parameters for the same fiber in an ordinary concrete mix. For the 12/0.4 mm fiber, τ_o is approximately twice what is found for same size steel fibers in ordinary concretes and is very similar to what was found in the dense mix reported in Stang et al. [7] (Table 1). Comparing the water-to-powder ratio, r, in the different mixes it is found that $r = 0.18$ in the Densit material and $r = 0.25$ in the material described in Stang et al. [7] compared to $r = 0.35$ to 0.48 in the ordinary concrete mixes containing steel fibers.

It is interesting to note that the τ_o for brass-coated fibers even in the presence of the highly densified matrix remains at a similar level as for steel fibers in a

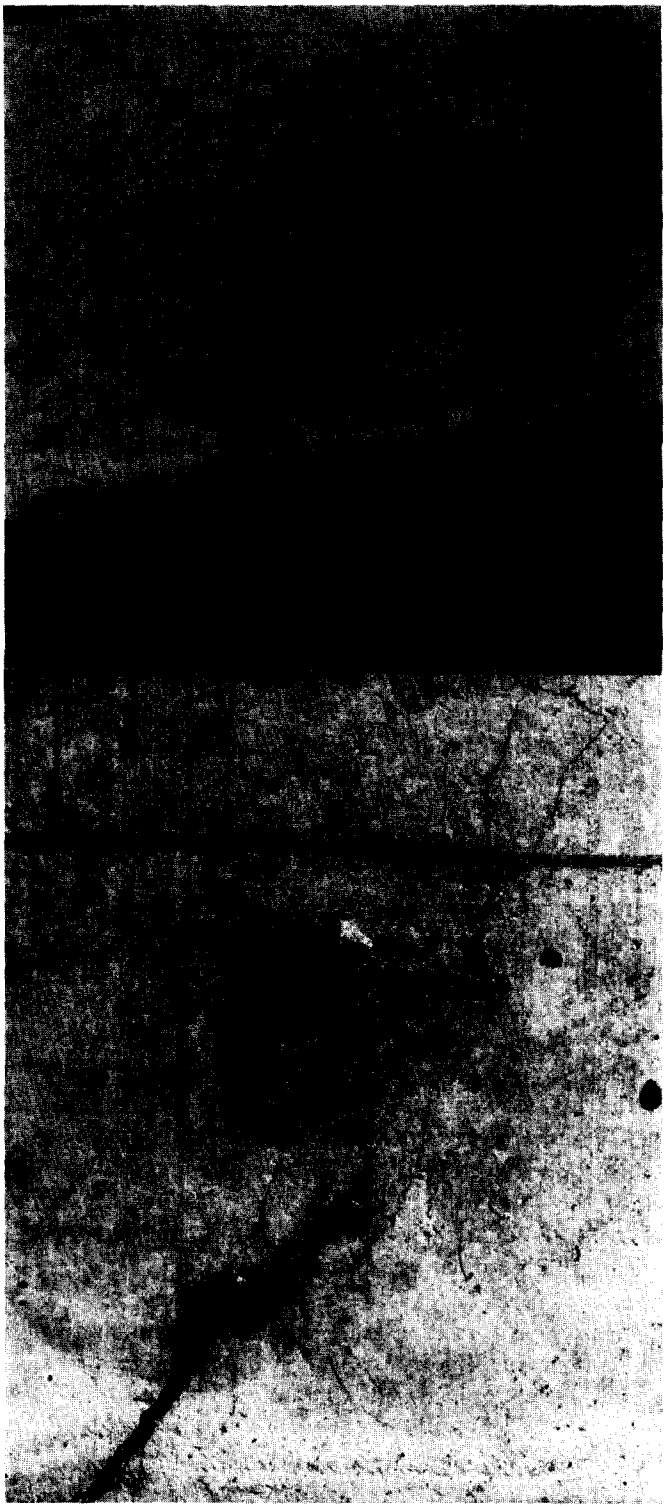

FIGURE 17. Matrix damage at hooked end of steel fiber. (a) Flexural crack in a steel FRC beam; (b) exposed hooked end after matrix spalled.

normal strength matrix. This may be due to the dissolution of the brass coating leading to a weak adhesive strength at the interface for this system. The change in color of the brass-coated fiber from a bright gold to a dull dark color provides circumstantial evidence for this argument.

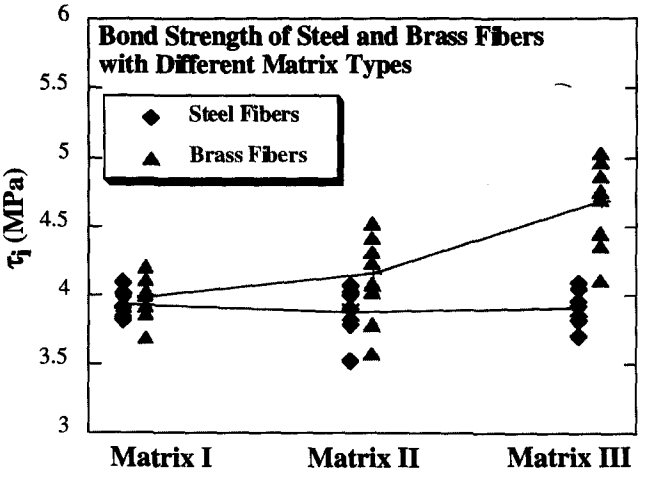

FIGURE 18. Effect of interface densification on steel and brass bond strengths [50].

The apparent discrepancy between the conclusions by Chan and Li [50] and the steel fiber reinforced Densit system might be due to the extent of modification in the interface in the various matrices. While densification of the ITZ is observed by ESEM in the system studied [50], the main change may be confined to the microstructure of the ITZ material. In the Densit material, it is possible that both microstructure density in the transition zone and the contact surface area with the fiber increased, leading to enhancement of adhesion and ITZ strength. For this system, therefore, densification does lead to interfacial bond strength increase. (Curiously, the slip-

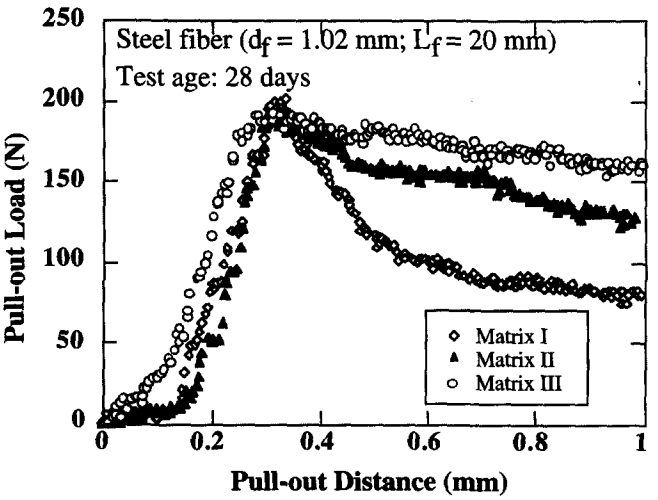

FIGURE 19. Pull-out test results of straight steel fibers in various matrices. No change in peak load is detected, despite confirmation of densification in the interface transition zone [50].

TABLE 4. Mix proportions for fiber concretes (composite tensile tests in Table 1)

Component	[6]	[6]	[7]	OB-10	ZB-05	8500	Fatigue-5
Cement	340	465	320	445	445	390	500
Microsilica	34	35	41	44	44	35	—
Fly ash	—	100	—	—	—	100	—
Clay	—	—	17	—	—	—	—
Sand	1090	780	896	1027	1027	840	810
Gravel	730	420	1014	698	698	560	810
Plasticizer	—	3	—	—	—	3	—
Superplasticizer	2.5	8	25	3.0	3.0	7.3	20
Water	158	253	95	170	170	215	238
Pp. fiber	—	10-30	—	—	—	10	10
S. st. fiber 12.5/0.4	—	—	78/234	—	—	—	—
S. st. fiber 25/0.4	39-157	—	—	78.4	—	—	—
H. st. fiber 30/0.5	—	—	—	—	39.2	75	75

Note: S. st. = straight steel; h. st. = hooked steel; pp. = polypropylene. Numbers in table refer to kg/m^3.

softening parameter a_1 deduced for the Densit matrix and normal matrix remains at −4.0, whereas the system studied in Chan and Li [50] reveals a reduced weakening effect in the denser matrix, as evidenced in Figure 19).

The trend of bond increase with matrix densification in the Densit composite system correlates with trends indicated by recent single stainless steel fiber pull-out experiments [55] in a densified small particle (DSP) system (r = 0.18) matrix similar to the Densit matrix described above. In that study, Shannag et al. [55] found that the frictional bond strength was 4.4 MPa for the DSP system compared to 1.9 MPa for ordinary strength mortar determined under similar conditions. Similar to the findings by Chan and Li [50], the densified system also reveals a more gentle decay with slip in the post-peak (sliding after full debond) in comparison with the ordinary strength mortar.

Increase of bond strength was also found in carbon fiber/cement interfaces when densification of the matrix was achieved by addition of microsilica and/or lowering the water-to-binder ratio. Using a microfiber pull-out testing devise, Katz et al. [56] determined that the interfacial bond increases by 54% (from 0.52 to 0.8 MPa) when the water-to-binder ratio changes from 0.50 to 0.35, and increases by 95% (from 0.52 to 1.29 MPa) when the matrix was further densified by the addition of 10% microsilica.

Another technique to achieve densification of the porous ITZ is by the addition of polymers. The wall effect partially responsible for the porous nature of the ITZ creates an inefficient packing of cement particles around the fiber. By coating the cement grains, the polymer can lubricate them and enhance their packing density, an idea popularized by the pioneering work of Birchall et al. [57] on macro-defect-free cement. Recent work by Najm et al. [58] and Chu et al. [59] revealed a 60% to 80% increase in bond strength of a steel fiber in a cement matrix when polyvinyl alcohol (PVA) was added at a dosage of 1.4% by weight (of cement). A dense, fine-grained, and ductile ITZ at the interface was observed. The authors attributed the morphology and property changes in the ITZ to the following additional or complementary mechanisms in addition to the cement grain lubrication and packing effect:

(1) Increase in the ductile polymer concentration near the fiber hydrophilic surface due to diffusion of the molecularly dispersed PVA through the liquid when the cement paste is mixed. Coating of the fiber surface by a monomolecular PVA film is possible.
(2) Inhibition of the more open structured calcium hydroxide (CH) crystals from forming on the fiber surface and enhancement of the nucleation of calcium silicate hydrate (CSH).
(3) Formation of a polymeric network around cement grains, which may lead to improvement in microdamage tolerance and ITZ material ductility.

TABLE 5. Typical Densit mix containing 6 vol.% of steel fibers, Dramix OL 12/0.4 (from Nielsen [53])

Component	Fraction by Weight (%)	Amount* (kg/m^3)	Density (kg/m^3)
Cement	27.2*	753	3150
Microsilica	6.8*	188	2250
Superplasticizer	—*	—	—*
Quartz 0–0.25 mm	7	194	2640
Quartz 0.25–1 mm	12	332	2640
Quartz 1–4 mm	24	664	2670
Water	6	166	1000
Steel fibers (6 vol.%)	17	471	7500

Note. When changing the fiber content, adjustments are typically made in the contents of quartz sand. The numbers marked with an asterisk are slightly inaccurate since no information was given on the contents or type of superplasticizer or the air content.

TABLE 6. Overview of the types of reinforcement used in the investigation by Nielsen [53]

Dramix Fiber Type	Length (mm)	Diameter (mm)	Tensile Strength (MPa)	Notes	V_f Tested (%)
OL 6/0.15 HC	6	0.15	2950	Brass coated	3,6,9
OL 13/0.15 HC	13	0.15	2950	Brass coated	3
OL 12/0.4	12	0.40	1350		3,6,9

Thus, the effect of PVA addition on ITZ appears to be a combination of physical densification in addition to changes in the organic, inorganic, and organic/inorganic phase microstructures. However, Chu et al. [59] found that PVA has little influence on bond properties of polypropylene fiber, which has low energy or hydrophobic surfaces.

Wei et al. [45] and Mandel et al. [60] also used polymer to achieve steel fiber/matrix bond enhancement. In that case, they added 15% by weight of acrylic polymer particles of 50- to 100-nm size. The fourfold increase in bond strength appears to have been achieved with densification of the ITZ by gap grading between the smaller polymer particles and the cement grains. This mechanism is similar to that using clay or microsilica as microfillers.

It appears that improvement in interfacial bond due to densification depends on a number of factors:

(1) The size of the microfillers. For the materials described above, the microfiller size ranges from molecular size to micron size (Table 8), amounting to one to several orders of magnitude smaller than cement grain size, which is typically 10 to 20 μm;
(2) The chemical nature of the fiber surface, which governs the concentration of microfiller additives at the ITZ, and also governs the relative adhesive strength to the cohesive strength of the material inside the porous ITZ zone; and
(3) The physical and/or chemical interactions between the additive and the cement paste material near the ITZ, as exemplified by the PVA effect on CH crystal inhibition and polymer network creation around cement grains.

TABLE 7. Overview of bonding parameters used in prediction of post-cracking peak stress for the different fiber types

Dramix Fiber Type	τ_0 (MPa)	a_1 (MPa/mm)	a_2 (MPa/mm^2)
OL 6/0.15 HC	3.5	−4.0	0.0
OL 13/0.15 HC	3.5	−4.0	0.0
OL 12/0.4	7.0	−4.0	0.0

Because these factors are activated to different extents in the various fiber/cement systems described, it is perhaps not surprising that different degrees of effectiveness of densification on interfacial bond are found in these investigations. In addition, it is possible that the additive (either in the form of inert microfiller or chemically active additive) may alter the free shrinkage of the ITZ and surrounding bulk material. As discussed in the previous section, matrix shrinkage can strongly influence the frictional bond of the fiber/matrix interface.

Surface Modification

Cold gas plasma has been used commercially to enhance adhesion between plastic parts in manufacturing processes. This technology was recently applied to alter interfacial bond characteristics in polymeric fibers/epoxy matrix systems [61] and in polymeric fibers/cementitious matrix systems [62]. In the presence of a gas plasma, hydrogen atoms are removed from the polymer backbone and replaced by polar groups. The specific polar group is related to the type of gas used. The presence of polar functional chemical groups on the fiber surface enhances reactivity and thus improves the adhesion between fiber and cement. In addition, wettability of the fiber surface by cement can be enhanced, leading to increased contact between fiber and the surrounding cementitious matrix. (Wettability improvement can be confirmed by contact angle measurement.) As a result, it may be expected that the fiber surface abrasion effect described earlier becomes more significant.

The effect of plasma treatment on the interface bond

TABLE 8. Size of microfiller additives

Microfiller Additives	Size	Reference
Cement grain	10–20 μm	[44,65]
Clay	1 μm	[52]
Microsilica	0.1 μm	[53,56]
Fly ash*	10–20 μm	[65]
Acrylic polymer particles	50–100 nm	[45]
PVA molecules	Molecular size < 1 nm	[59]

Note. For comparison, the average size of cement grains is also given.
*Fly ash included as a common concrete additive.

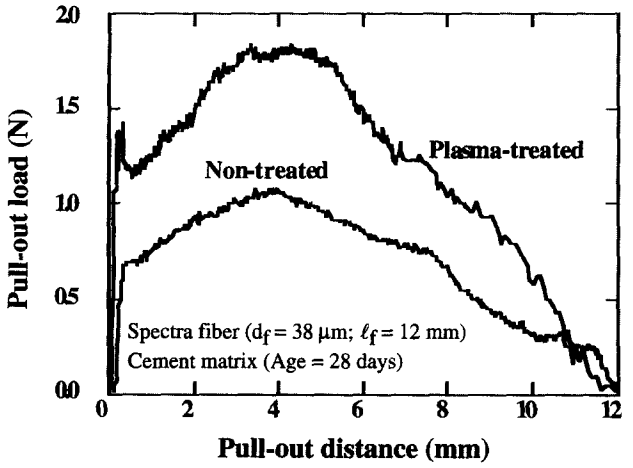

FIGURE 20. Effect of surface modification of polyethylene fiber by plasma treatment on pull-out behavior [62].

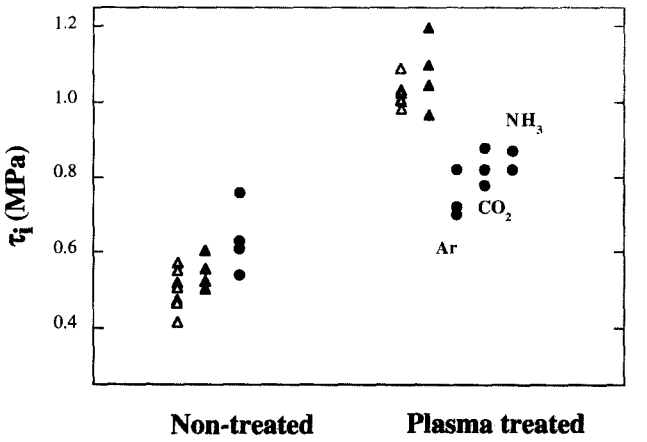

FIGURE 21. Effect of plasma treatment on frictional bonds of spectra fiber/cement. Closed triangles are bond strength deduced from pull-out test; closed circles are bond strength deduced from composite tensile test; open circles indicate cement matrix without microsilica [62].

properties of polyethylene fibers in cement was studied by Li et al. [62] based on both single fiber pull-out test and uniaxial tensile test of composites. Figure 20 shows the pull-out test results of a polyethylene fiber treated with an argon plasma gas, with a flow rate of 40 ml/min, 100 W of power, and 5 minutes of treatment duration. A cement paste with w/c ratio of 0.4 serves as the matrix material. For comparison, pull-out test results of an identical untreated fiber are also shown. In both cases, the pull-out curves show the characteristics of a polymeric fiber. Full interface debonding is followed by a slip-hardening behavior associated with surface abrasion, observed for both fibers after pull-out.

It is clear that the load at the end of debonding (indicated by the first load drop) is almost doubled, reflecting a bond strength increase from 0.55 to 1.06 MPa due to plasma treatment. For the case of the plasma-treated fiber, the load drop at the end of debonding indicates that chemical bonding may have occurred, and that this chemical bond strength seems to have exceeded the initial frictional bond. Thereafter, the effect of abrasion on the plasma-treated fiber appears to be more significant than that on the untreated fiber, indicated by the more rapid rise in load with pull-out distance.

Figure 21 summarizes bond strength deduced from single fiber pull-out tests and from composite tests, for matrices with and without microsilica, and for various types of plasma gas treatment. The composite test result indicates a less dramatic rise in bond property in comparison to the pull-out test. Even so, it is evident that plasma treatment is effective in fiber surface modification for bond enhancement.

The enhanced effect of surface abrasion due to plasma treatment is even stronger in a polypropylene fiber treated under the same conditions as for the polyethylene fiber [25]. For the polypropylene fiber, the initial bond value τ_0 appears to be only marginally improved (about 20%). However, the amount of slip hardening is significantly enhanced over that of the untreated fiber (Figure 22). Microstructural observations under ESEM reveal different interfacial microstructure on the contact surface after the fibers are carefully peeled off, suggesting improved wettability of the polypropylene fiber to cement solution and alteration of the physical nature of the contact surface. Plasma treatment seems to have a stronger effect on the coefficients a_1 and a_2 in eq 4 for the polypropylene fibers than the polyethylene fibers.

The magnitude of bond improvement by plasma

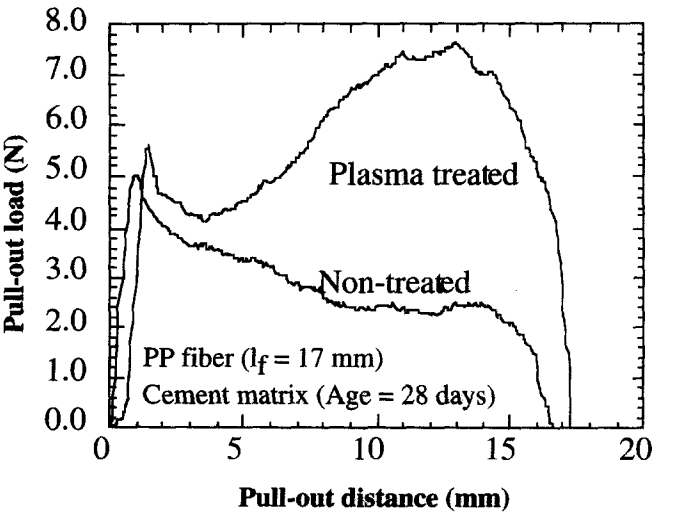

FIGURE 22. Effect of surface modification of polypropylene fiber by plasma treatment on pull-out behavior [25].

treatment is dependent on the chemical composition of the gas used, the power intensity, and treatment time, among other factors. When these factors are optimized for a given fiber type, it is expected that bond strength can be enhanced by several fold. The most recent data from the University of Michigan [63] indicate the possibility of achieving a sixfold increase in bond strength.

Other forms of surface modification techniques, such as Corona treatment, co-extrusion, or surface coating, have been carried out on a variety of fibers. However, much of this information is proprietary to the fiber manufacturer, and information on such modification effect on fiber/cement matrix interface bond strength is not readily available.

Conclusions

From Table 3 and the discussions above, it is clear that all three classes of strengthening mechanisms—fiber deformation, interface densification, and fiber surface modification—can lead to substantial improvement in interfacial bond strength and/or slip-hardening behavior. The magnitude of bond increase appears highest in fiber deformation—several times up to a factor of 28—although the high end of this number represents an "effective bond" when the hooked end of the steel fiber is activated and also depends on the matrix strength to withstand the anchorage stress of the hooked end. Fiber deformation technique in bond strength improvement is available for the highly deformable fibers such as polymer and steel, but has not been applied to carbon or other brittle fibers. In addition, the fiber deformation technique has generally been limited to the larger diameter fibers, or because of the deformation technique itself, the fiber diameter becomes larger (such as by twisting polymer filaments together). This limits its contribution to certain composite properties that relate inversely to fiber diameter.

The interface densification technique provides bond strength enhancement up to several times, but is limited to metal and carbon fibers only. For the low surface energy polymer fibers, apart from the fiber deformation technique mentioned above, fiber surface modification such as by plasma treatment has been demonstrated to be effective in improving interface bond strength up to a factor of several fold, and also induces slip hardening in the post-debonding stage. These techniques may be regarded as complementary rather than exclusive, and may be combined to reach new levels of bond strength improvement. For example, the interface densification technique using PVA depends on the chemical reactivity of the fiber surface. Since plasma treatment can bring about higher surface reactivity by means of selective polar group introduction, it will be natural to expect that the PVA densification technique ought to be effective even for polymeric fibers when combined with plasma treatment. This combined technique is being demonstrated at the University of Michigan.

The interface strengthening mechanisms reviewed in this article also suggest that fiber deformation, interface densification, and plasma treatment can all lead to modification of the coefficients in the slip-dependent friction constitutive relation. In some cases, slip hardening is achieved or further enhanced.

If Coulomb friction provides a primary component to interfacial friction, as discussed earlier in this article, an additional means of enhancing interfacial bond could be to deliberately introduce residual shrinkage stress and, therefore, clamping pressure on the fiber by the surrounding matrix. For example, the use of cement with large shrinkage as a fiber coating may be effective. These avenues of interface property improvement may be worth pursuing.

Despite extensive research on interface characterization, property measurement, and microstructural studies, the detailed understanding of the underlying mechanisms of interface behavior and the conversion of this knowledge into useful techniques for interface property improvements, and therefore composite property tailoring, remain wide open. Future research will need to focus systematically on these issues, recognizing the different effectiveness of fiber deformation, interface densification, fiber surface modification, and their combinations on bond improvement of different fiber types in cementitious composites.

Acknowledgments

This review article is largely based on work carried out at the ACE-MRL at the University of Michigan and at the Technical University of Denmark. Research support by the U.S. National Science Foundation to the University of Michigan (MSS-9301949) is gratefully acknowledged. Collaborative research between the University of Michigan and the Technical University of Denmark has been supported by the International Partnership Program, Rackham Graduate School at the University of Michigan, and by the NATO International Scientific Exchange Programmes, Collaborative Research, grant no. 930023. V.C.L. acknowledges helpful discussions with R. Robertson on polymer admixture influence on ITZ and with H.C. Wu on plasma treatment on fiber/matrix interface behavior.

References

1. Bentur, A.; Wu, S.T.; Banthia, N.; Baggott, R.; Hansen, W.; Katz, A.; Leung, C.K.Y.; Li, V.C.; Mobasher, B.; Naaman, A.E.; Robertson, R.; Soroushian, P.; Stang, H.; Taerwe, L.R. In *High Performance Fiber Reinforced Cementitious Composites*; Naaman, A.E.; Reinhardt, H., Eds.; Chapman and Hall: London, 1995; pp 149–191.
2. Bentur, A. In *Materials Science of Concrete, Vol. I*; Skalny, J., Ed.; The American Ceramic Society Inc.: Westerville, OH, 1989; pp 223–284.

3. Gray, R.; Johnston, C.D. *Proceedings RILEM Symposium*, Lancaster, **1978,** 317–328.
4. Stang, H. In *Fracture of Brittle, Disordered Materials: Concrete, Rock and Ceramics*. Baker, G.; Karihaloo, B.L., Eds.; E&FN Spoon: London, 1995; pp 131–148.
5. Li, V.C. *ASCE J. Mater. Civil Eng.* **1992,** *4*, 41–57.
6. Li, V.C.; Stang, H.; Krenchel, H. *Mater. Struct.* **1993,** *26*, 486–494.
7. Stang, H.; Li, V.C.; Krenchel, H. *J. Mater. Struct.* **1995,** *28*, 210–219.
8. Stang, H.; Shah, S.P.; *J. Mater. Sci.* **1986,** *21*, 953–957.
9. Gao, Y.C.; Mai, Y.W.; Cotterell, B. *J. Appl. Math. Phys.* **1988,** *39*, 550–572.
10. Leung, C.K.Y. *ASCE J. Eng. Mech.* **1992,** *118*, 2298–2318.
11. Shah, S.; Ouyang, C. *J. Amer. Ceram. Soc.* **1991,** *74*, 2727–2738, 2947–2953.
12. Mobasher, B.; Ouyang, C.; Shah, S.P. *Internat. J. Fract.* **1991,** *50*, 199–219.
13. Palmer, A.C.; Rice, J.R. *Proc. R. Soc. Lond. A* **1973,** *332*, 527.
14. Rice, J.R. *ASME J. Appl. Mech.* **1968,** *35*, 379–386.
15. Shao, Y.; Li, Z.; Shah, S.P. *J. Adv. Cem. Based Mater.* **1993,** *1*, 55–66.
16. Li, V.C.; Chan, Y.W. *ASCE J. Eng. Mech.* **1994,** *120*, 707–719.
17. Stang, H.; Li, Z.; Shah, S.P. *J. Eng. Mech.* **1990,** *116*, 2136–2150.
18. Leung, C.K.Y.; Li, V.C. *J. Mater. Sci.* **1991,** *26*, 5996–6010.
19. Leung, C.K.Y.; Li, V.C. *J. Mater. Sci. Lett.* **1990,** *9*, 1140–1142.
20. Aveston, J.; Cooper, G.A.; Kelly, A. In *The properties of fibre composites*. Conference Proceedings. National Physical Laboratory, 4 November 1971; IPC Science and Tech. Press, Ltd; Guildford, Surrey, England, 1971; pp 15–26.
21. Li, V.C.; Maalej, M. *J. Cem. Concr. Compos.* **1996,** *18*, 239–249.
22. Maalej, M.; Li, V.C. *ASCE J. Civil Eng. Mater.* **1994,** *6*, 390–406.
23. Wang, Y.; Li, V.C.; Backer, S. *Internat. J. Cem. Compos. Lightweight Concr.* **1988,** *10*, 143–149.
24. Geng, Y.; Leung, C.K.Y. *J. Mater. Sci.* **1996,** *31*, 1285–1294.
25. Chan, Y.W. *Doctoral Thesis*; University of Michigan: Ann Arbor, MI, 1995.
26. Naaman, A.E.; Namur, G.G.; Alwan, J.M.; Najm, H.S. *J. Struct. Eng.* **1991,** *117*, 2769–2790.
27. Leung, C.K.Y.; Geng, Y. *ASTM J. Testing and Evaluation* **1997,** *25*; In press.
28. Leung, C.K.Y.; Geng, Y. *J. Compos. Eng.* **1995,** *5*, 1331–1348.
29. Pinchin, D.J.; Tabor, D. *J. Mater. Sci.* **1978,** *13*, 1261–1266.
30. Kim, J.K.; Zhou, L.M.; Mai, Y.W. *J. Mater. Sci.* **1993,** *28*, 3923–3930.
31. Li, V.C.; Mishra, D.K.; Naaman, A.E.; Wight, J.K.; LaFave, J.M.; Wu, H.C.; Inada, Y. *J. Adv. Cem. Based Mater.* **1994,** *1*, 142–149.
32. Stang, H. *Adv. Cem. Based Mater.* **1996,** *4*, 106–115.
33. Krenchel, H. U.S. Patent No. 4,261,754, April 14, 1981; British Patent No. 16.05004, February 17, 1982; French Patent No. 78 13 173, November 19, 1984.
34. Krenchel, H. *Developments in Fiber Reinforced Cement and Concrete, RILEM Symposium*, 1986, pp 333–338.
35. Krenchel, H.; Jensen, H.W. In *Fibrous Concrete*. Proceedings of the Symposium on Fibrous Concrete, London, 1980; The Construction Press: Lancaster, 1980; pp 87–98.
36. Naaman, A.E.; Shah, S.P.; Throne, J.L. *Proceedings of the ACI International Symposium on Fiber Reinforced Concrete*, **1984,** 375–396.
37. Li, V.C.; Wang, Y.; Backer, S. *J. Compos.* **1990,** *21*, 132–140.
38. Banthia, N. *Can. J. Civil Eng.* **1990,** *17*, 610–620.
39. Banthia, N.; Trottier, J. *ACI Mater. J.* **1994,** *91*, 435–446.
40. Stang, H.; Aarre, T. *Cem. Concr. Compos.* **1992,** *14*, 143–154.
41. Hansen, S.; Stang, H. *Report 305, Department of Structural Engineering, Technical University of Denmark*, 1993.
42. Stang, H.; Jun, Z. *Recent Advances in Experimental Mechanics*; A.A. Balkema: Rotterdam, Netherlands, 1994, pp 1347–1352.
43. Rasmussen, T.V. *Ph.D. Thesis*; Technical University of Denmark: Lyngby, 1997.
44. Bentur, A. In *Advances in Cementitious Materials*; Mindless, S., Ed.; The American Ceramic Society: USA, 1991; pp 523–547.
45. Wei, S.; Mandel, J.A.; Said, S. *ACI Mater. J.* **1986,** *83*, 597–605.
46. Kawamura, M.; Igarashi, S. *Proceedings ACI Special Publication on Interface Fracture and Bond*, 1995.
47. Mehta, P.K.; Gjorv, O.E. *Cem. Concr. Res.* **1982,** *12*, 585–595.
48. Ping, X.; Beaudoin, J.J. *Cem. Concr. Res.* **1992,** *22*, 597–604.
49. Bentur, A.; Cohen, M.D. *J. Am. Ceram. Soc.* **1987,** *70*, 738–743.
50. Chan, Y.W.; Li, V.C. *J. Adv. Cem. Based Mater.* **1997,** *5*, 8–17.
51. Glavind, M. *Ph.D. Thesis*; Technical University of Denmark: Lyngby, 1992.
52. Glavind, M.; Stang, H. *Brittle Matrix Compos.* **1991,** *3*, 508–518.
53. Nielsen, C.V. *Ph.D. Thesis*; Technical University of Denmark, Danish Academy of Technical Sciences: Lyngby, 1995.
54. Aarre, T. *Report Series R, No. 301, Department of Structural Engineering, Technical University of Denmark*, 1992.
55. Shannag, M.J.; Hansen, W.; Brincker, R. *Mater. Res. Soc. Symp. Proc.* **1995,** *370*, 507–517.
56. Katz, A.; Li, V.C.; Kazmer, A. *J. Mater. Civil Eng.* **1995,** *7*, 125–128.
57. Birchall, J.D.; Howard, A.J.; Kendall, J. *Nature (Lond)* **1981,** *289*, 388–390.
58. Najm, H.; Naaman, A.E.; Chu, T.J.; Robertson, R.E. *J. Adv. Cem. Based Mater.* **1994,** *1*, 115–121.
59. Chu, T.J.; Robertson, R.E.; Najm, H.; Naaman, A.E. *J. Adv. Cem. Based Mater.* **1994,** *1*, 122–130.
60. Mandel, J.A.; Wei, S.; Said, S. *ACI Mater. J.* **1987,** *84*, 101–109.
61. Hild, D.N.; Schwartz, P. *J. Adhes. Sci. Technol.* **1992,** *6*, 879–896.
62. Li, V.C.; Wu, H.C.; Chan, Y.W. *J. Amer. Ceram. Soc.* **1996,** *79*, 700–704.
63. Wu, H.C.; Li, V.C. *UMCEE Report No. 95-20*, 1995.
64. Naaman, A.E.; Shah, S.P. *ASCE J. Struct. Div.* **1976,** *102*, 1537–1548.
65. Mehta, P.K. *Concrete, Structures, Properties, and Materials*; Prentice Hall: New Jersey, 1986.
66. Li, V.C.; Wang, Y.; Backer, S. In *Materials Research Society Symposia Volume 114: Bonding in Cementitious Composites*; Mindess, S.; Shah, S., Eds., **1988,** 167–174.